JOURNAL OF APPLIED ELECTROCHEMISTRY **28** (1998) 89–95

Deposition of Zn–Co by constant and pulsed current

A. STANKEVIČIŪTĖ, K. LEINARTAS, G. BIKULČIUS, D. VIRBALYTĖ, A. SUDAVIČIUS, E. JUZELIŪNAS*

Institute of Chemistry, Goštauto 9, 2600 Vilnius, Lithuania

Received 18 September 1996; revised 21 July 1997

The initial stages of both Zn–Co and Zn electrodeposition were investigated by electrochemical quartz crystal microgravimetry (EQCM). The initial electrode mass growth, determined under both pulse and constant current conditions, was much higher than predicted by Faraday's law. This was explained in terms of the precipitation of scarcely soluble compounds of zinc on an electrode surface. The EQCM data confirm that the hydroxide suppression mechanism explains the anomalous Zn and Co codeposition. A nonuniform adsorption of brightener (benzalaceton) on the profiled surface was concluded on the basis of plating distribution investigations. The additive adsorbs to a greater extent on the surface projections.

Keywords: *zinc*, *cobalt*, *alloy*, *electrodeposition*, *interphase layer*, *electrochemical quartz crystal microgravimetry*

1. Introduction

Zn–Co alloys containing small amounts of Co (usually less than 1%) are widely used for corrosion protection. The corrosion resistance of alloyed coatings is significantly higher than that of conventional zinc coatings [1–4]. Compared with pure zinc, the coatings also have other superior properties, for instance, hardness, ductility, internal stress, paintability and weldability.

The inhibiting action of the alloying additive is not well understood. The inhibition was attributed to chemical stabilization of the oxide film and/or to a retardation of transport of ions or vacancies within the passive layer that has developed on the surface during corrosion [5]. According to [6], corrosion inhibition is due to the elimination by cobalt of the negatively charged Zn cation vacancies.

Electrodeposition of Zn–Co alloys was characterized by Brenner as anomalous codeposition [7] because deposition of the less noble component Zn is preferential. The anomalous deposition was observed at higher current densities [8–10], whereas at low currents the deposition was normal [8]. The codeposition was found to be anamalous even at Zn(II)/Co(II) ratios significantly lower than 1; however, the process became normal with increasing electrolysis time [11].

Various explanations for anomalous codeposition are given in the literature. An underpotential deposition hypothesis was proposed [12], according to which the deposition of components proceeds continuously on an alloy surface that is different from the parent metals. It is possible that continuous underpotential deposition of the less noble component takes place and is, therefore, preferential.

Mathias and Chapman [13] and Landolt [14] attributed anomalous codeposition to certain types of kinetic behaviour, as well as to the difference in the exchange current densities of the components. An inhibited deposition of the alloying additive was explained in terms of the retardation effect of zinc hydroxide which is included in the alloy matrix [15].

The hydroxide suppression mechanism was suggested by Dahms and Croll in their discussion anomalous codeposition iron-nickel alloys [16]. The anomalous Zn–Co codeposition was also explained in terms of a zinc hydroxide suppression mechanism [8]. Hydrogen evolution and, consequently, a rise in pH in the vicinity of the cathode occurs during electrolysis. If the pH rises sufficiently, precipitation of zinc hydroxide and its adsorption on the surface take place. The hydroxide film prevents Co deposition, whereas Zn deposits readily from the adsorbed layer. Therefore, Zn acts as if it were a more noble component of the system.

Recently, the hydroxide oscillation concept was proposed [17], according to which the thickness of the hydroxide layer changes periodically. H^+ and Co preferential deposition takes place when the hydroxide layer is depleted. The pH increase due to rapid hydrogen reduction leads to reformation of the layer and codeposition becomes anomalous.

Thus, the existing interpretations of the mechanism are equivocal and need to be supported by additional arguments. In the present study Zn–Co deposition was investigated by the electrochemical quartz crystal microbalance (EQCM) technique. Since EQCM supplies very sensitive data about electrode mass changes *in situ*, the formation of a hydroxide film can be successfully investigated. Attention focused on initial deposition stages on gold and zinc substrates.

* Author to whom correspondence should be addressed.

0021-891X

Pulse electrolysis is applied to deposit many metals and alloys from aqueous, nonaqueous and molten salt electrolytes. The superior properties of Zn–Co alloys obtained by pulse plating were reported by Paatsch [18] and Grünwald *et al.* [4]. A smoother surface, lower porosity and higher corrosion resistance were observed. This influence of pulse plating on microdistribution of Zn–Co coatings on profiled substrates was investigated in the present study.

2. Experimental details

2.1. *Electrolytes*

The plating bath used was analogous to that in [4] (Table 1). Many properties of Zn–Co coatings from the above bath have been reported [4]. For instance, alloys deposited by pulse current contain $\leqslant 0.21\%$ Co and the corrosion resistance of the coatings is more than twice as high as that of pure zinc.

2.2. *Electrodes*

High-purity zinc (99.999) was used to prepare the working electrode for voltammetric measurements. A sample (surface area 1 cm^2) was pressed into a PTFE holder. The metal surface was polished with a fine-grain abrasive paper treated with a mixture of MgO and CaO (weight ratio 1 : 1) and rinsed in triple-distilled water. The samples were visually smooth and bright. A copper rotating disc electrode was pressed into a Teflon jacket. The working surface was 0.2 cm^2. The disc was zinc-coated from a slightly acidic plating bath before measurements. The reference electrode was a saturated Ag/AgCl/KCl electrode and a platinum foil served as a counter electrode.

W-shaped surfaces were used for plating distribution investigations (Fig. 1). The samples were prepared using pieces (60 mm × 10 mm × 2 mm) of carbon steel. All experiments were conducted using surfaces with profile heights, $H_{a,0}$, of 26 μm and step distances, S, of 1000 μm (Fig. 1). The profile angle was approximately 170°. A more detailed description of the surface preparation procedure is reported elsewhere [19]. The Zn–Co coatings were plated with a current density of 15 mA cm^{-2} and the thickness was 10 μm (the electrolysis duration followed the data in [4]).

Table 1. Composition of the chloride–sulphate plating bath used for Zn and Zn–Co electrodeposition

Compound	*Amount*/g dm^{-3}
$ZnSO_4.7\,H_2O$	70
$CoSO_4.7\,H_2O$	30
KCl	150
H_3BO_3	20
Sodium benzoate	4
Zinc acetate	6
Polyethylene glycol (m. weight 4000)	6
Benzalaceton (BA) (5% in alcohol)	4 ml dm^{-3}
	pH 5.0

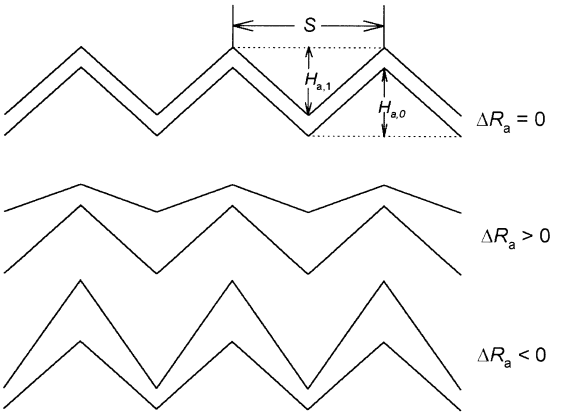

Fig. 1. Characteristics of surface profiles.

2.3. *Equipment*

EQCM measurements were conducted using quartz discs (produced by Quarzverarbeitung, Neckarbischofsheim, Germany), their fundamental frequency being $f_0 = 5$ MHz, and $r = 15$ mm. Both quartz sides were plated with gold 200 nm thick using the standard vacuum thermal evaporation technique. The geometric area of the working electrode was 0.78 cm^2. To improve the compactness of the layer, a 1 μm gold coating was deposited from a gold plating bath. The EQCM device has been described elsewhere [20].

A PI 50 potentiostat coupled with a Pr 8 signal programmer was used as a pulsed current source. The same apparatus was used to carry out voltammetric measurements. The fast potential–time dependencies were recorded by a C 8–13 memory oscilloscope.

The cobalt content was determined by atomic absorption spectroscopy after dissolution of the coatings in 1 M HCl. A Perkin Elmer 603 machine was used for this purpose. Zn–Co coatings 10 μm thick were deposited on a copper basis ($S = 2$ cm^2).

The distribution of the elements in the zinc surface layers was investigated by X-ray photoelectron spectroscopy (XRPS). The spectra were recorded by Escalab MK spectrometer using X-radiation of MgK_α (1253.6 eV, pass energy of 20 eV). The samples were etched in the preparation chamber with ionised argon at a vacuum of 5×10^{-9} mPa. An accelerating voltage of about 1 kV and a beam current of 50 μA were used. The etching rate was 2 nm min^{-1} with a beam current of 20 μA. Both inlet and exit slits of the analyser were 1.5 mm in diameter, which made it possible to analyse the spot in the middle of the sample in the etching area. Each sample was scanned three times. Peaks of Zn $2p_{3/2}$, Au $4f_{7/2}$, O 1s, Co $2p_{3/2}$ were recorded.

2.4. *Estimation of plating microdistribution*

The plating microdistribution was characterised by the parameter $\Delta R_a = R_{a,0} - R_{a,1}$, where $R_{a,0}, R_{a,1}$ are

the mean deviation of profile from the middle line within the studied distance (l) for the substrate and for the coating, respectively. This can be expressed as

$$R_{a,1} = \frac{1}{l}\int_0^l |y(x)|\mathrm{d}x \qquad (1)$$

where x is the abscissa of the profile and $y(x)$ the function which describes the profile. The R_a parameters were measured by a 252-profilograph–profilometer (Russia). It should be noted that the apparatus determines the mean R values, thus eliminating irregular extremes. The radius of the measurement needle was $10 \pm 2.5\,\mu$m. The distribution parameters were calculated from 16 measurements.

The value ΔR_a is negative when the projections are coated to a greater extent than the profile depth (Fig. 1). By contrast, ΔR_a is positive when coating primarily deposits in the profile depth. In the case of an ideal distribution the relations $R_{a,0} = R_{a,1}$ and $\Delta R_a = 0$ hold.

3. Results and discussion

3.1. *Dependence of Co concentration in the coatings on various factors*

Figure 2 shows potential vs time dependencies recorded during galvanostatic pulse polarization. The duration of the pulse was 10 ms, which is the same as in the case of the pulse plating studied (Table 2, Figs 6–8). The establishment time of quasi steady-state polarization values (τ_1) is relatively short ($\tau_1 \approx 2$–3 ms). The relaxation time after the current perturbation (τ_2) is rather longer ($\tau_2 \approx 15$ ms). Neither of the times τ_1 and τ_2 actually depend on the current densities applied.

Table 2 shows the results of an analysis of cobalt concentration in the coatings (c_{Co}). The coatings were placed both by constant and by pulse currents. The pulse duration was $t_i = 10$ ms and the durations of breaks were $t_p = 10$ and 50 ms. The coatings were 10 μm thick. Benzalaceton (BA) is used as a brightener in zinc electroplating processes [21–23]. Even a small amount of this additive drastically increases the electrode polarization [24]. The influence of BA on c_{Co} was investigated (Table 2).

Table 2. Values of c_{Co}(%) found in the coatings plated by constant and pulse current from the plating bath in Table 1 with and without BA

	Constant current	$t_i = t_p$ *= 10* ms	t_i *= 10* ms, t_p *= 50* ms
BA-containing bath	0.13	0.17	0.35
BA-free bath	0.2	0.25	0.37

The following conclusions may be drawn: (i) c_{Co} in the pulse plated coatings is higher than that in the coatings plated by constant current; (ii) an increase in t_p favours c_{Co} growth; (iii) BA leads to a decrease in c_{Co}; (iv) c_{Co} rises when the depositing current is increased.

It has already been mentioned that codeposition of cobalt with zinc by constant current is anomalous because deposition of the less noble component Zn is preferential. The codeposition under pulse plating conditions is also anomalous. The ratio of Co to Zn contents in the pulse plated coatings (Table 2) is much lower than the analogous ratio in the solution (Table 1), i.e. deposition of the less noble zinc is preferential.

3.2. *EQCM measurements*

EQCM can supply important information about mass changes occurring *in situ* during Zn–Co electrodeposition. This method is based on a linear relationship between changes in quartz oscillation frequencies and in electrode mass. According to [25], a theoretical proportional coefficient between these parameters is approximately 18 ng s cm^{-2} when the main resonance frequency is 5 MHz.

Figures 3, 4 and 6 depict the results of EQCM investigations. Frequency–time dependencies obtained under constant current conditions (Figs 3 and 4)

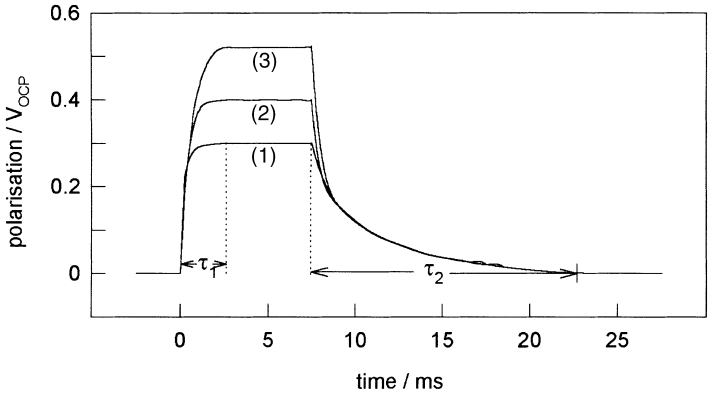

Fig. 2. Chronopotentiograms of Zn–Co deposition recorded during galvanostatic pulse polarization. Current densities: (1) 10, (2) 20, (3) 30 mA cm^{-2}. $E_{ocp} = -0.96$ V vs AgCl.

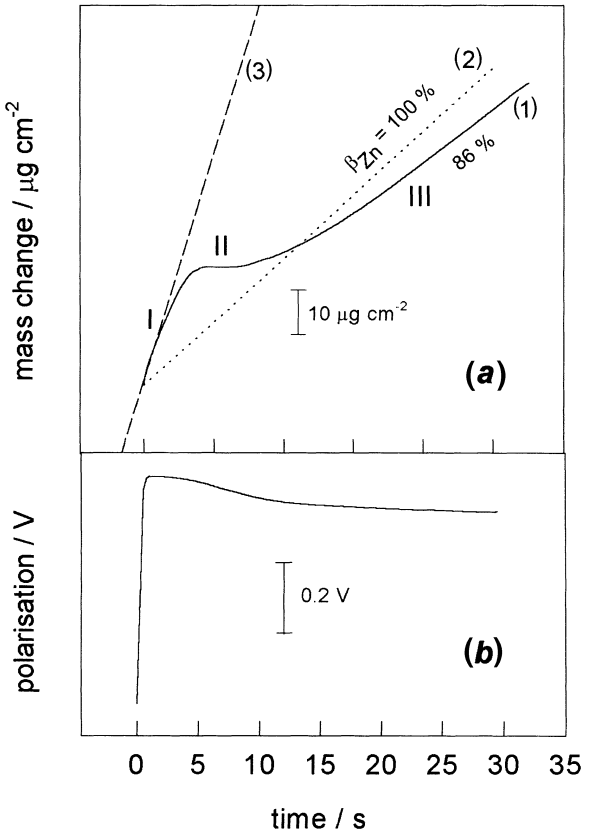

Fig. 3. (a) Electrode mass increase determined by EQCM during Zn–Co deposition on Au substrate. Depositing current density 9 mA cm^{-2}. (b) Electrode potential change vs open circuit potential. $E_{ocp} = -0.22$ V vs AgCl.

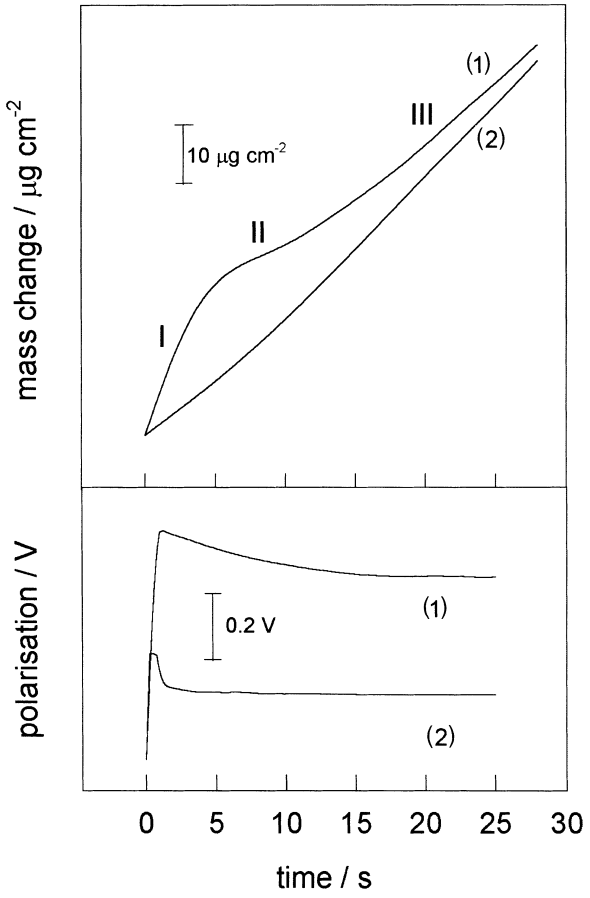

Fig. 4. (a) Electrode mass change determined by EQCM during Zn deposition on Au (1) and Zn (2) substrates. Bath composition as in Table 1 without $CoSO_4$; depositing current density 9 mA cm^{-2}. (b) Electrode potential change vs open circuit potential. E_{ocp}(V vs AgCl): (1) −0.16, (2) −0.78.

can be divided into the three following regions: (i) the rapid increase in mass which corresponds to 'current efficiency', $\beta \gg 100\%$; (ii) the termination (Fig. 3) or significant suppression (Fig. 4) of mass growth; (iii) the further mass growth which corresponds to current efficiency $\beta < 100\%$.

The following explanation of the above regularities proposed. A pH rise due to hydrogen evolution occurs in the vicinity of the cathode after switching on deposition current. The increase in pH is sufficient for zinc hydroxide precipitation, but low for the precipitation of Co hydroxide [8]. The preferential formation of the layer from Zn hydroxide takes place in the first region; therefore, the mass growth is much higher than predicted by Faraday's law assuming Zn–Co deposition. The repeated measurements (curve 2, Fig. 4) confirm the connection between the anomalously high mass growth and hydroxide layer formation. The hydroxide layer already existed on the surface before curve 2 was measured, because the layer formed in the course of the first curve. Evidently, the anomalously high mass growth in the case of curve 2 is not observed.

Observations reported in [17] support the above conclusion about hydroxide layer formation. Deposits were examined on the steel substrate by scanning electron microscopy after electrode polarization in a zinc plating bath. Only zinc hydroxide crystals were found on the substrate at lower cathodic polarizations, i.e. hydrogen evolution and zinc hydroxide precipitation were preferential to metal deposition.

The mass becomes constant (Fig. 3) or its growth is significantly suppressed (Fig. 4) when the hydroxide layer reaches its maximum thickness (regions II). The preferential hydrogen reduction occurs in the second region, and this actually does not affect the electrode mass. The third region corresponds to zinc deposition from the hydroxide layer, and also to simultaneous hydrogen reduction, which results in current efficiency $\beta < 100\%$.

The above data support the so-called hydroxide suppression mechanism of anomalous Zn and Co codeposition [8]. According to this mechanism, the deposition of Co(II) is inhibited because it proceeds through the Zn hydroxide layer. By contrast, deposition of zinc from the hydroxide layer is relatively fast. Thus, the higher nobility of cobalt is suppressed by the zinc hydroxide film.

The XRPS data show that oxygen is located in the surface layers of the sample (Fig. 5). The oxygen concentration decreases sharply approaching the Zn/Au interface. The surface analysed after 4 min etching does not actually contain oxygen, whereas the Zn concentration on the surface is higher than 40 at %. These data imply that zinc reduction from the oxide

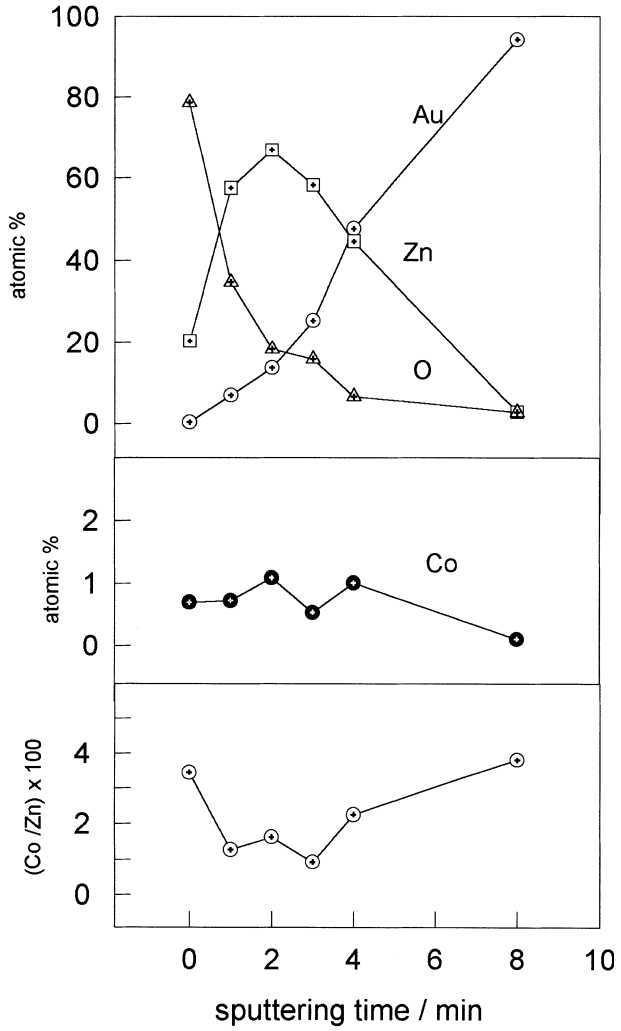

Fig. 5. Distribution of zinc, cobalt, oxygen and gold determined by XRPS in the layer deposited on Au substrate under conditions outlined in Fig. 3. The samples were etched with ionised argon. The lowest figure shows the change of concentration ratio c_{Co}(at %)/ c_{Zn}(at %) in the layer.

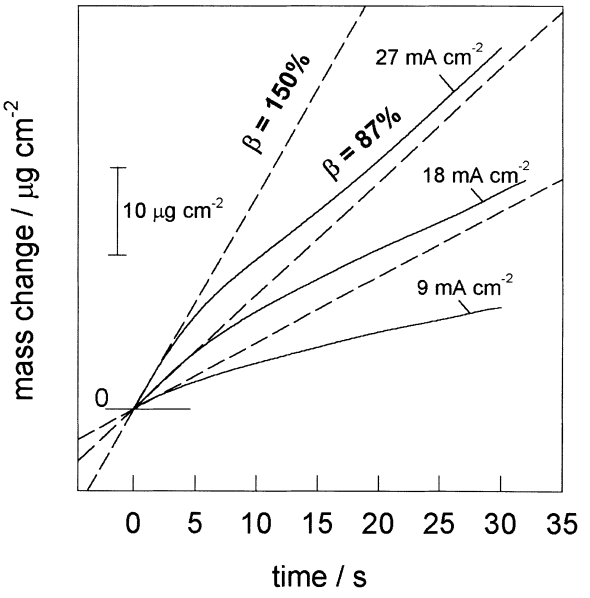

Fig. 6. Electrode mass increase determined by EQCM during Zn–Co pulse deposition ($t_i = 10$ ms, $t_p = 50$ ms) on the Zn–Co substrate. The Au surface has been preplated with Zn–Co coating before the measurements. Plating conditions: $t = 20$ s; $i = 9$ mA cm^{-2}.

layer proceeds without significant incorporation of oxygen into the alloy.

It should be noted that c_{Co} determined in the thin film (Fig. 5) is higher when compared to the analogous value determined in the relatively thick coating (Table 2). This may be accounted for by the different thickness of the hydroxide layer. The layer precipitated during the relatively short electrolysis time may be somewhat thinner and its suppression effect on Co codeposition may be less pronounced when compared to continuous electrolysis.

The XRPS data show a slight increase in the ratio c_{Co}/c_{Zn} when approaching the Zn/Au interface (Fig. 5). However, no significantly Co-enriched zone was found in the vicinity of this interface. Thus, the deposition was also anomalous in the first deposition stages. This is in agreement with the conclusion regarding hydroxide layer formation prior to alloy deposition.

The codeposition of Zn and Co under pulse plating conditions is also anomalous because the concentration of cobalt in the coatings is low (Table 2). The EQCM measurements show (Fig. 6) that the mass increase at the beginning of electrolysis is much higher than predicted by Faraday's law. In the course of electrolysis the dm/dt curves become rectilinear with the slope corresponding to the current efficiency $\beta < 100\%$ (Fig. 7). The anomalously high mass increase at the beginning of pulse electrolysis is indicative of the formation of a layer composed of scarcely soluble compounds. Thus, the hydroxide suppression mechanism appears to be a plausible explanation for anomalous Zn and Co codeposition even under pulse plating conditions.

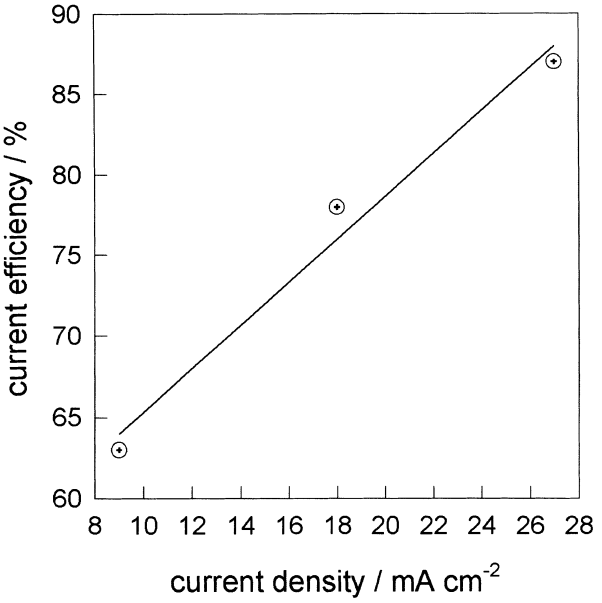

Fig. 7. Pulse current efficiency calculated from the rectilinear parts of the mass change dependencies in Fig. 6.

Two reasons can be proposed to explain interphase layer formation during pulse electrolysis: (i) precipitation of scarcely soluble compounds due to a pH increase occurring as a result of hydrogen evolution; (ii) formation of the layer during intervals between current pulses as a result of corrosion. The initial mass growth calculated for the upper curve in Fig. 6 corresponds to a 'current efficiency' of $\beta \approx 150\%$. To explain such mass growth as a result of the above corrosion, all the zinc deposited during the pulse must have been converted into $Zn(OH)_2$ during corrosion. This is unlikely because in this case the corrosion current should be comparable to the depositing current, that is, have an order of milliamps. However, the highest corrosion current in the system under study could be roughly estimated to within an order of microamps assuming the dissolved oxygen and H^+ ions act as the depolarizers [26]. Thus, the precipitation of scarcely soluble compounds during the current pulse is a resonable explanation for the anomalously high mass increase. To a certain extent the result is surprising because the duration of polarization was very short (10 ms) and, therefore, the layer with a pH gradient should be very thin.

3.3. *Plating microdistribution*

To study plating microdistribution coatings were deposited on the profiled substrates (Fig. 1) and the parameter ΔR_a was measured by profilograph–profilometer (Fig. 8). The difference $\Delta R_a = R_{a,0} - R_{a,1}$ is negative when the deposition on the projections is preferred. However, ΔR_a is positive in the case of primary deposition in the profile depth. In the case of an ideal plating distribution the values $R_{a,0}$ and $R_{a,1}$ are equal, that is $\Delta R_a = 0$.

In the brightener-free solution the values of ΔR_a were found to be negative for a constant current deposition (curve 5 in Fig. 8). This is indicative of preferred plating on the surface projections. Evidently, distribution improves in this solution when the pulse current is applied (curve 4). At the current densities of 10 and 30 mA cm^{-2} $\Delta R_a \approx 0$ is observed, that is, the plating distribution is close to ideal.

The presence of BA in the bath improves the plating distribution under constant current conditions (curve 3 in Fig. 8). Well distributed coatings were also attained in solution containing BA by the pulse current $i = 10$ mA cm^{-2}. However, at $i = 20$ and 30 mA cm^{-2} rather high ΔR_a values were observed indicating preferable deposition in the profile depth (curves 1 and 2). An increase in ΔR_a especially favours prolongation of the breaks between the pulses. These results suggest a non-uniform adsorption of BA on the profiled surface. The surface projections must be covered to a greater extent by additive and, therefore, the deposition in the profile depth is more favourable.

The following explanation for the curves in Fig. 8 is proposed. Adsorption of BA may be characterised by the degree of electrode covering (Θ). The greatest value of Θ is under open circuit conditions ($\Theta_{i=0}$). The degree of surface covering during electrolysis (Θ_i) is somewhat less because of a new metal phase formation, that is, it is true that $\Theta_{i=0} > \Theta_i$. The value of Θ_i during the pulse plating is higher than that during constant current plating because part of the newly deposited metal is covered during the intervals between pulses. An increase in intervals between pulses should favour an increase in Θ_i, i.e. Θ_i should approach $\Theta_{i=0}$. Thus, the surface coverage should decrease in the order $\Theta_{tp=50\ ms} > \Theta_{tp=10\ ms} > \Theta_i$. If the preferable deposition on the projections is caused

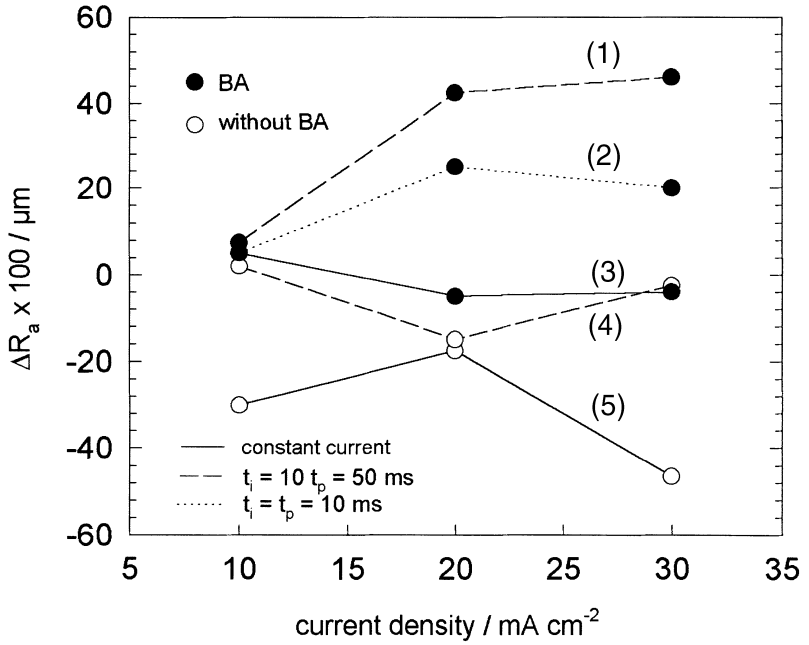

Fig. 8. Parameter ΔR_a determined for Zn–Co coatings deposited on profiled substrates.

by nonuniform BA adsorption, the value of ΔR_a should also decrease in the above order. The data in Fig. 8 confirm such a tendency. This result once again shows that BA adsorbs to a greater extent on the surface projections.

4. Conclusions

The initial stages of Zn–Co deposition on gold were investigated by EQCM. The mass change dependencies recorded under constant current conditions can be divided into the following three regions: (i) the rapid mass increase which is much higher than predicted by Faraday's law for Zn–Co deposition; (ii) the termination or the significant suppression of mass growth; (iii) the rectilinear increase in mass which corresponds to the current efficiency $\beta < 100\%$. The anomalously high mass growth in the first region was explained in terms of precipitation of zinc hydroxide on the surface which occurs as a result of hydrogen evolution and, consequently, of pH rise in the cathode vicinity. The hydrogen evolution mainly occurs in the second region. Zinc reduction from the hydroxide layer proceeds in the third region.

The initial increase in electrode mass during pulse electrolysis is also significantly higher than predicted by Faraday's law assuming Zn–Co deposition. Formation of a layer from scarcely soluble compounds of zinc is also probable in this case. EQCM data confirm that the hydroxide suppression mechanism explains anomalous Zn and Co codeposition by constant current and pulse current. A study of the plating microdistribution suggests a nonuniform adsorption of the brightner, benzalaceton, on the profiled surface. The additive adsorbs to a greater extent on the surface projections, therefore, Zn–Co deposition in the profile depth is favourable.

References

[1] T. Adaniya, M. Omura, K. Matsudo and H. Naemura, *Plat. Surf. Finish.* **68** (1981) 96.
[2] E. Knaak, H. Köhler and J. Hadley, *Metalloberfläche* **39** (1985) 139.
[3] W. Siegert and J. Hadley, *ibid.* **43** (1989) 78.
[4] E. Grünwald, A. Ziman, Cs. Várhelyi and Cs. Juhos, *Galvanotechnik* **85** (1994) 3274.
[5] J. R. Vilche, K. Jüttner, W. J. Lorenz, W. Kautek, W. Paatsch, M. H. Dean and U. Stimming, *J. Electrochem. Soc.* **138** (1989) 3773.
[6] W. Kautek, M. Sahre and W. Paatsch, *Electrochim. Acta* **39** (1994) 1151.
[7] A. Brenner, 'Electrodeposition of Alloys', Vol. 1, Academic Press, New York (1963), p. 75.
[8] K. Higashi, H. Fukushima, T. Urakawa, T. Adaniya and K. Matsudo, *J. Electrochem. Soc.* **128** (1981) 2081.
[9] R. Fratesi and G. Roventi, *Mater. Chem. Phys.* **23** (1989) 529.
[10] H.-M. Wang and T. J. O'Keefe, *J. Appl. Electrochem.* **24** (1994) 900.
[11] E. Gómez and E. Vallés, *J. Electroanal Chem.* **397** (1995) 177.
[12] M. J. Nicol and H. I. Philip, *ibid.* **70** (1976) 233.
[13] M. F. Mathias and T. W. Chapman, *J. Electrochem. Soc.* **134** (1987) 1408.
[14] D. Landolt, *Electrochim. Acta* **39** (1994) 1075.
[15] Yu. M. Loshkarev, V. I. Korobov, V. V. Trofimenko and F. A. Chmilenko, *Protection of Metals* **30** (1994) 79.
[16] H. Dahms and I. M. Croll, *J. Electrochem. Soc.* **112** (1965) 771.
[17] H. Yan, J. Downes, P. J. Boden and S. J. Haris, *ibid.* **143** (1996) 1577.
[18] W. Paatsch, *Metalloberfläche* **41** (1987) 39.
[19] G. Bikulčius, E. Juzeliūnas, A. Stankevičiūtė, *J. Adv. Mater.* **4** (1996) 80.
[20] E. Juzeliūnas, P. Kalinauskas, P. Miečinskas, *J. Electrochem. Soc.* **143** (1996) 1525.
[21] *US Patent* 3 808 110 (1974).
[22] *British patent* 2 160 223 A (1988).
[23] L. Grincevičienė, G. Bernotienė, D. Mockutė and S. Jakobson, *in* 'Materials of 9th meeting of Lithuanian electrochemists', Vilnius (1983), p. 93.
[24] A. Stankevičiūtė, K. Leinartas and E. Juzeliūnas, unpublished data.
[25] G. Sauerbrey, *Z. Phys.* **155** (1959) 206.
[26] H. Kaesche, 'Die Korrosion der Metalle', Springer-Verlag, Berlin (1990).